




STAR FORMATION

Teutsch 76: A deep near-infrared study

SAURABH SHARMA^{1,*} , LOKESH DEWANGAN², NEELAM PANWAR¹,
HARMEEN KAUR³, DEVENDRA K. OJHA⁴, RAMKESH YADAV⁵, AAYUSHI VERMA¹,
TAPAS BAUG⁶, TIRTHENDU SINHA⁶, RAKESH PANDEY², ARPAN GHOSH¹ and
TARAK CHAND¹

¹Aryabhata Research Institute of Observational Sciences (ARIES), Manora Peak, Nainital 263001, India.

²Astronomy and Astrophysics Division, Physical Research Laboratory (PRL), Navrangpura, Ahmedabad 380009, India.

³Center of Advanced Study, Department of Physics, DSB Campus, Kumaun University, Nainital 263002, India.

⁴Tata Institute of Fundamental Research (TIFR), Homi Bhabha Road, Colaba, Mumbai 400005, India.

⁵National Astronomical Research Institute of Thailand (NARIT), Chiang Mai 50200, Thailand.

⁶Satyendra Nath Bose National Centre for Basic Sciences (SNBNCBS), Block-JD, Sector-III, Salt Lake, Kolkata 700106, India.

*Corresponding author. E-mail: saurabh@aries.res.in

MS received 18 November 2022; accepted 8 February 2023

Abstract. We have performed a detailed analysis on the Teutsch 76 (T76) open cluster using the deep near-infrared (NIR) observations taken with the TANSPEC instrument mounted on the 3.6m Devasthal optical telescope along with the recently available high quality proper motion data from the Gaia data release 3 and deep photometric data from Pan-STARRS1 survey. We have found that the T76 cluster is having a central density concentration with circular morphology, probably due to the star-formation processes. The radius of the T76 cluster is found to be 45'' (1.24 pc) and 28 stars within this radius were marked as highly probable cluster members. We have found that the cluster is located at a distance of 5.7 ± 1.0 kpc and is having an age of 50 ± 10 Myr. The mass function slope (Γ) in the cluster region in the mass range of $\sim 0.75 < M/M_{\odot} < 5.8$ is estimated as -1.3 ± 0.2 , which is similar to the value of -1.35 given by [Salpeter \(1955\)](#). The cluster is not showing any signatures of mass-segregation and is currently undergoing dynamical relaxation.

Keywords. Star cluster—star formation—stellar evolution.

1. Introduction

As most of the stars form in a clustered environment in molecular clouds, the dynamics of stars in the clusters as well as the structure of clusters measured as a function of cluster age hold important clues on the processes of star formation and stellar evolution ([Lada & Lada 2003](#)). Many clusters show the distribution of massive stars toward their central region of clusters and whether this segregation of massive stars occurs due to an evolutionary effect or is of primordial origin, is not yet entirely clear.

Most of the studies related to the stellar evolution and dynamics on star clusters during the past decade are not always based on deep photometric data and lack the membership determination based on high-quality proper motion (PM) data. Teutsch 76 open cluster (α_{J2000} : $22^{\text{h}}28^{\text{m}}44^{\text{s}}.2$, δ_{J2000} : $+61^{\circ}37'52''$) ([Kronberger et al. 2006](#)), hereafter T76, cf. Figure 1), one of the poorly studied open clusters, is located in the galactic plane towards the 2nd Galactic quadrant ($l = 106^{\circ}.8171$, $b = +03^{\circ}.3082$). This cluster is located in the eastern part of the Sharpless region ‘Sh 2–141’ inside a mid-infrared (MIR) bubble seen in WISE MIR band image (cf. Figure 1). The Sh 2–141 HII region is reported to be ionized by an O8V star (named as ‘S1’ hereafter) ([Russeil et al. 2007](#)). We

This article is part of the Special Issue on “Star formation studies in the context of NIR instruments on 3.6m DOT”.

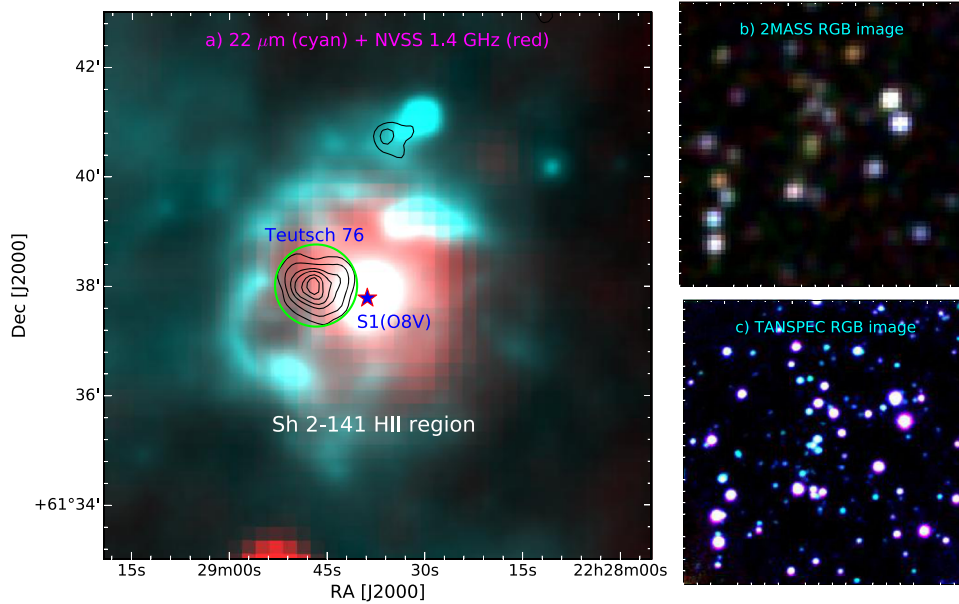


Figure 1. Left panel: Color-composite image obtained using the NVSS 1.4 GHz (red) and WISE 22 μm (cyan) images for an area of $\sim 15 \times 15$ arcmin² around the T76 cluster. The black contours are the isodensity contours generated using nearest neighbor method from the 2MASS data (cf. Section 3.1). The green circle encloses the cluster T76 region. Right panels: Comparison of the color-composite images obtained by using the J (blue), H (green) and K (red) images of the T76 cluster from the 2MASS (top panel) and TANSPEC observations (bottom panel).

have performed a detailed analysis on this cluster to understand its dynamical evolution by using our deep near-infrared (NIR) observations taken from the TIFR-ARIES Near-infrared Spectrometer (TANSPEC; Sharma *et al.* 2022) recently installed on the 3.6m telescope at Devasthal, Nainital, India (Kumar *et al.* 2018), along with the recently available data from the Gaia data release 3 (Gaia Collaboration *et al.* 2016, 2018) and Panoramic Survey Telescope and Rapid Response System (Pan-STARRS1) (Chambers *et al.* 2016).

In this paper, Section 2 describes the observations and data reduction. The structure of this cluster, membership probability of stars in the cluster region, fundamental parameters (i.e., age and distance) of the cluster and mass function (MF) analyses are presented in Section 3. The dynamical structure of this cluster is discussed in Section 4 and we conclude our studies in Section 5.

2. Multi-wavelength data sets

2.1 Deep NIR data

The central region of the T76 open cluster (refer Section 3.1) was observed in the NIR J (1.20 μm), H (1.65 μm) and K (2.19 μm) bands (cf. Figure 1) during the nights of 19 and 27 November 2020 using the TANSPEC instrument mounted at the Cassegrain main port of the 3.6m ARIES Devasthal Optical Telescope (DOT). The weather conditions in these nights

were good with relative humidity $< 50\%$ and the full-width at half maxima of the stellar images was typically ~ 0.7 arcsec in J band. The field-of-view (FOV) of the TANSPEC is $\sim 60 \times 60$ arcsec square with a plate scale of 0.244 arcsec. The observations were taken in seven dither positions with 135 frames, each having 20 s of exposure. Thus, the total exposure time was 45 min in each of the bands. Dark and sky flats were also taken during the observations. Sky frames in each filter were generated by median combining the dithered frames.

The basic data reduction including image cleaning, photometry and astrometry, is done using the standard procedure explained in Sharma *et al.* (2020). We transformed our instrumental JHK magnitudes into a standard Vega system by using the following transformation equations:

$$(J - H) = (0.94 \pm 0.11) (j - h) - (0.02 \pm 0.08), \quad (1)$$

$$(J - K) = (0.78 \pm 0.08) (j - k) - (0.51 \pm 0.14), \quad (2)$$

$$(J - j) = (-0.03 \pm 0.06) (J - H) - (2.54 \pm 0.03), \quad (3)$$

where the capital JHK are the standard magnitudes of the stars taken from the 2MASS catalog and the small jhk are the present instrumental magnitudes of the same stars normalized per second exposure time. The DAOPHOT errors as a function of corresponding standard magnitudes are shown in Figure 2. We have used only those stars for further analyses, which are having signal-to-noise ratio > 10 (photometric errors

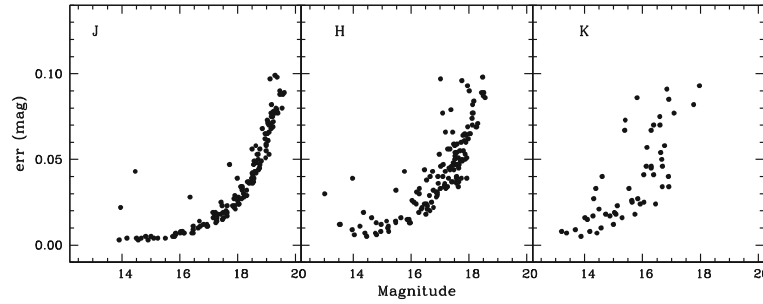


Figure 2. DAOPHOT errors as a function of J , H and K magnitudes.

<0.1 mag). In total, 143 stars were identified in the T76 cluster with detection limits of 19.6 mag, 18.6 mag and 18.0 mag in J , H and K bands, respectively. Figure 1 shows the comparison of a 2MASS image with the TANSPEC image. We can clearly see the resolved and faint stars in TANSPEC observations. Some of the brighter stars (3 in total) were saturated in our observations; we have taken their respective magnitudes from the 2MASS point source catalog.

2.2 Archival data

To study a wider area around T76, we have selected a FOV of 15×15 arcmin square as shown in Figure 1 and downloaded the available data from different surveys, i.e., Gaia DR3¹ (Gaia Collaboration *et al.* 2016, 2018), the Pan-STARRS1 or PS1 data release² (Chambers *et al.* 2016) and the 2MASS point source catalog³ (Cutri *et al.* 2003). For our analyses, we have used only those sources, which have photometric uncertainties <0.1 mag.

3. Results and analysis

3.1 Structure of T76 cluster

To study the structure of T76 open cluster, we obtained stellar number density maps for the sample of stars taken from the 2MASS survey covering 15×15 arcmin square FOV around this cluster region. The stellar number density maps were generated using the nearest neighbor (NN) method as described by Gutermuth *et al.* (2005). We took the radial distance necessary to encompass the sixth nearest stars and computed the local surface density in a grid size of 5 arcsec (cf. Gutermuth *et al.*

2009). The stellar number density contours derived by this method are plotted in Figure 1 as black curves. The lowest contour is 1σ above the mean of stellar density ($13 \text{ stars arcmin}^{-2}$) and the step size is equal to 1σ ($3.5 \text{ stars arcmin}^{-2}$). As can be seen from the contours, the cluster is almost circular and is located within the Sh 2–141 HII region near a massive star S1 (O8V) (Russeil *et al.* 2007; Foster & Brunt 2015, cf. Figure 1). The approximate boundary of the T76 cluster is shown with a green circle in Figure 1. The radius of the T76 cluster is found to be $45''$ centered at α_{2000} : $22^{\text{h}}28^{\text{m}}46^{\text{s}}.68$, δ_{J2000} : $+61^{\circ}38'01''.2$ (cf. Figure 1).

3.2 Membership probability

Gaia DR3 has opened up the possibility of an entirely new perspective on the problem of membership determination in cluster studies by providing the new and precise parallax measurements up to very faint limits⁴ (Gaia Collaboration *et al.* 2016, 2018). Gaia proper motion (PM) data located within the cluster region (cf. Section 3.1, radius $<45''$) and having PM error $\sigma_{\text{PM}} < 3 \text{ mas yr}^{-1}$ are used to determine membership probability of stars located in this region. PMs, μ_x , i.e., $\mu_{\alpha} \cos(\delta)$ and μ_y i.e., μ_{δ} , are plotted as vector-point diagrams (VPDs) in the panel-1 of Figure 3 (left panel). The panel-2 show the corresponding $G_{(330-1050 \text{ nm})}$ vs. $G_{\text{BP}(330-680 \text{ nm})} - G_{\text{RP}(630-1050 \text{ nm})}$ Gaia color-magnitude diagrams (CMDs). The left sub-panels show all stars, while the middle and right sub-panels show the probable cluster members and field stars. A circular area of a radius of 1 mas yr^{-1} (keeping in mind the errors and the expected dispersion in the PM of cluster stars) around the cluster centroid in the VPD of PMs has been selected visually to define our membership criterion. The chosen radius is a compromise between losing cluster members with poor PMs and including field stars sharing mean PM. The CMD of the

¹<https://gea.esac.esa.int/archive/>.

²<http://catalogs.mast.stsci.edu/>.

³<http://tdc-www.harvard.edu/catalogs/tmpsc.html>.

⁴<https://gea.esac.esa.int/archive/>.

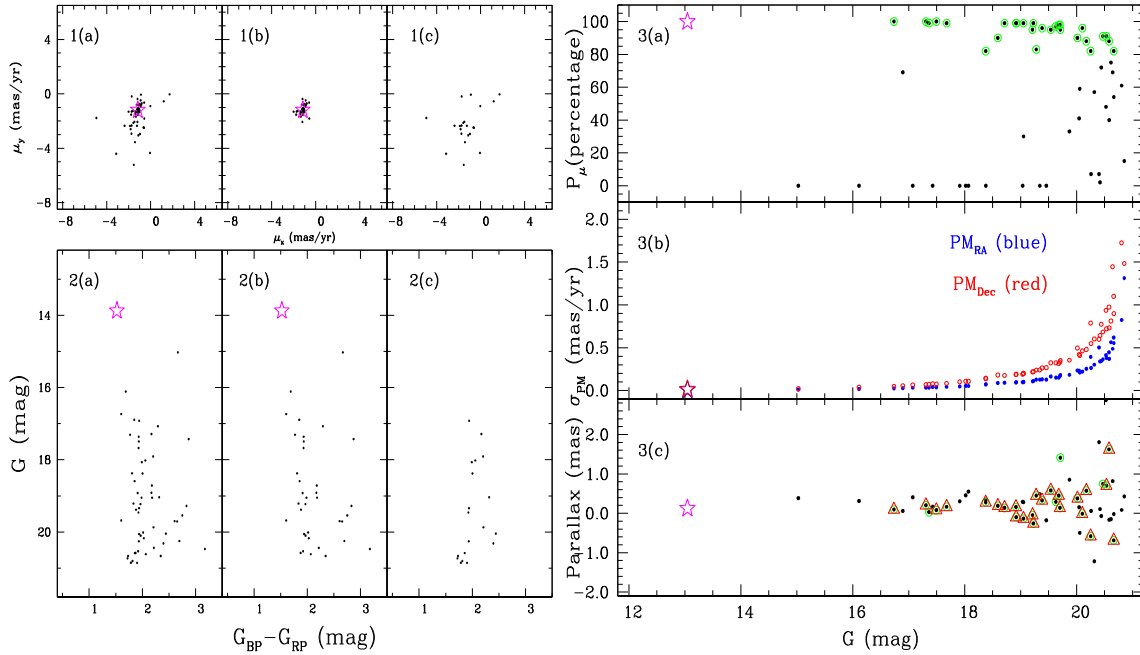


Figure 3. PM vector-point diagrams (VPDs; panel-1) and G vs. $(G_{BP} - G_{RP})$ CMDs (panel-2) for the stars located inside the T76 cluster region (cf. Section 3.1, radius $<45''$). The left sub-panels show all stars, while the middle and right sub-panels show the probable cluster members and field stars. Panel-3: Membership probability P_μ , PM errors σ_{PM} and parallax of stars as a function of G magnitude for stars in the cluster region. The probable member stars ($P_\mu > 80\%$) are shown by green circles, while the 24 members used for distance estimation of the T76 cluster are shown by red triangles (see text for details). Location of massive star S1 (O8V) is also shown in all panels by a star symbol.

most probable cluster members are shown in the lower-middle sub-panel. The lower-right sub-panel represents the CMD for field stars. Few cluster members are visible in this CMD because of their poorly determined PMs. The tight clump centering at $\mu_{xc} = -2.4$ mas yr $^{-1}$, $\mu_{yc} = -1.1$ mas yr $^{-1}$ and radius = 1 mas yr $^{-1}$ in the top-left sub-panel represents the cluster stars, and a broad distribution is seen for the probable field stars. Assuming a distance of ~ 5 kpc (cf. Section 3.3) and a radial velocity dispersion of 1 km s $^{-1}$ for open clusters (Girard *et al.* 1989), the expected dispersion (σ_c) in PMs of the cluster would be ~ 0.04 mas yr $^{-1}$. For remaining stars (probable field stars), we have calculated: $\mu_{xf} = -2.65$ mas yr $^{-1}$, $\mu_{yf} = -2.14$ mas yr $^{-1}$, $\sigma_{xf} = 2.53$ mas yr $^{-1}$ and $\sigma_{yf} = 1.29$ mas yr $^{-1}$. These values are further used to construct the frequency distributions of cluster stars (ϕ_c^v) and field stars (ϕ_f^v) by using the equations given in Yadav *et al.* (2013) and then, the value of membership probability (ratio of distribution of cluster stars with all the stars) of all the stars within the T76 cluster (Section 3.1, radius $<45''$), is given by using the following equation:

$$P_\mu(i) = \frac{n_c \times \phi_c^v(i)}{n_c \times \phi_c^v(i) + n_f \times \phi_f^v(i)}, \quad (4)$$

where n_c ($=0.55$) and n_f ($=0.45$) are the normalized number of stars for the cluster and field ($n_c + n_f = 1$), respectively. The membership probability estimated as above, errors in the PM and parallax values are plotted as a function of G magnitude in panel-3 of Figure 3. As can be seen in this plot, a high membership probability ($P_\mu > 80\%$) extends down to $G \sim 20$ mag. At brighter magnitudes, there is a clear separation between cluster members and field stars supporting the effectiveness of this technique. Errors in PM become very large at faint limits and the maximum probability gradually decreases at those levels. Except few outliers, most of the stars with high membership probability ($P_\mu > 80\%$) are following a tight distribution. Finally, from the above analysis, 28 stars were considered as members of the T76 cluster based on their high membership probability, $P_\mu (>80\%)$.

3.3 Distance and age of cluster

We have calculated the mean of the reported photo-geometric distances of 24 members of the T76 cluster (Bailer-Jones *et al.* 2021) (leaving a couple of outliers, as shown in Figure 3 with red triangles) as $\sim 5 \pm 1$ kpc. The previous spectro-photometric measurements

Table 1. Parameters for T76/Sh 2–141.

References	V_{LSR} (km s $^{-1}$)	Kinematical distance (kpc)	Spectrophotometric distance (kpc)	A_V (mag)	Ionizing star/age
This work	–	–	5.7 ± 1.0	3.95	50 Myr
Green et al. (2019)	–	–	–	3.94	–
Kim et al. (2018)	–	–	–	3.75	–
Kharchenko et al. (2016)	–	–	3.5	3.95	8 Myr
Anderson et al. (2015)	–62.9 (X-band, 9 GHz, 3 cm)	7 ± 1.2	–	–	–
Foster & Brunt (2015)	–65.8 (^{12}CO) to –62.9 (HI)	–	9.92 ± 1.98	3.90	O8V
Russeil et al. (2007)	–64.4	–	8.34 ± 0.6	4.46	O8V
Pineault & Joncas (2000)	–65 (CO) ^a to –63.8 (H α) ^b	7	–	–	O8

^aFich & Blitz (1984); ^bFich et al. (1990).

place this cluster at different distances ($\sim 3.5\text{--}10$ kpc, cf. Table 1). The ionizing source of the Sh-141 H II region, i.e., ‘S1’, an O8V star, is also located at a farther distance of $6.4^{+0.8}_{-0.4}$ kpc ([Bailer-Jones et al. 2021](#)). The reported kinematical distance of the molecular cloud containing the T76 cluster and the Sh 2-141 H II region is 7 ± 1.2 ([Pineault & Joncas 2000](#); [Anderson et al. 2015](#)). The distances to clusters with mean parallaxes smaller than ~ 0.2 mas (distance ≥ 5 kpc) are better constrained by classical isochrone fitting methods (e.g., [Phelps & Janes 1994](#); [Sharma et al. 2006, 2017, 2020](#); [Pandey et al. 2020a, b, 2022](#)). Therefore, to further check the validity of PM distance estimation of T76 ($\sim 5 \pm 1$ kpc), we have used the PS1 g vs. $(g - y)$ CMD for the stars in the cluster region along with the member stars as shown in Figure 4(a). The index $(g - y)$ has been used here because of having a very large color range. We have also shown the ZAMS derived from [Pastorelli et al. \(2019\)](#) corrected for extinction and distance values reported earlier, i.e., ($A_V = 3.95$ mag, distance = 3.5 kpc; [Kharchenko et al. 2016](#)) and ($A_V = 4.46$ mag, distance = 8.34 kpc; [Russeil et al. 2007](#)). Clearly, both sets of these parameters do not fit to cluster stars distribution in the CMD. In Figure 4(b), we show similar CMD, but fitted with $A_V = 3.95$ mag ([Kharchenko et al. 2016](#); [Green et al. 2019](#)) and distance = 5 kpc (mean distance of cluster members), 6.4 kpc (distance of a massive star ‘S1’) and 5.7 kpc (black curve, CMD best fitted value). The distance of 5.7 kpc is estimated from the visually fit of ZAMS to the lower envelope of the distribution of member stars, where the bend occurs in the MS (see for details, [Golay 1974](#); [Phelps & Janes 1994](#)). Clearly, out of these three ZAMSs corrected for different distance estimates, the member stars are best represented by a ZAMS corrected for a distance of 5.7 kpc. The massive star ‘S1’ also represented

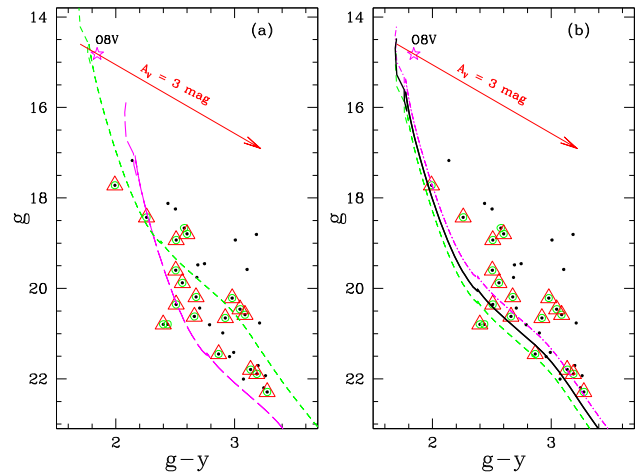


Figure 4. (a) PS1 g vs. $(g - y)$ CMD for the stars in the cluster region (black dots). The green circles are the member stars of the cluster. The curves denote a ZAMS derived from [Pastorelli et al. \(2019\)](#) corrected for extinction and distance values reported earlier, i.e., ($A_V = 3.95$ mag, distance = 3.5 kpc, [Kharchenko et al. 2016](#), green dashed curve) and ($A_V = 4.46$ mag, distance = 8.34 kpc, [Russeil et al. 2007](#), magenta dashed curve). (b) Same as panel (a), but for CMD fitted with $A_V = 3.95$ mag ([Kharchenko et al. 2016](#); [Green et al. 2019](#)) and distance = 5 kpc (magenta curve, mean distance of cluster members), 6.4 kpc (green curve, distance of massive star ‘S1’) and 5.7 kpc (black curve, CMD fitted value).

best by this distance estimate as it can be traced back to ZAMS along with reddening vector to the intrinsic color of O8V spectral type star (cf. Figure 4b). Here, it is worthwhile to note that the visual fitting in this case is prone to large error as the cluster can have differential reddening due to nebulosity around it. Therefore, we have estimated the error in the distance as 1.0 kpc using the procedure outlined in [Phelps & Janes \(1994\)](#).

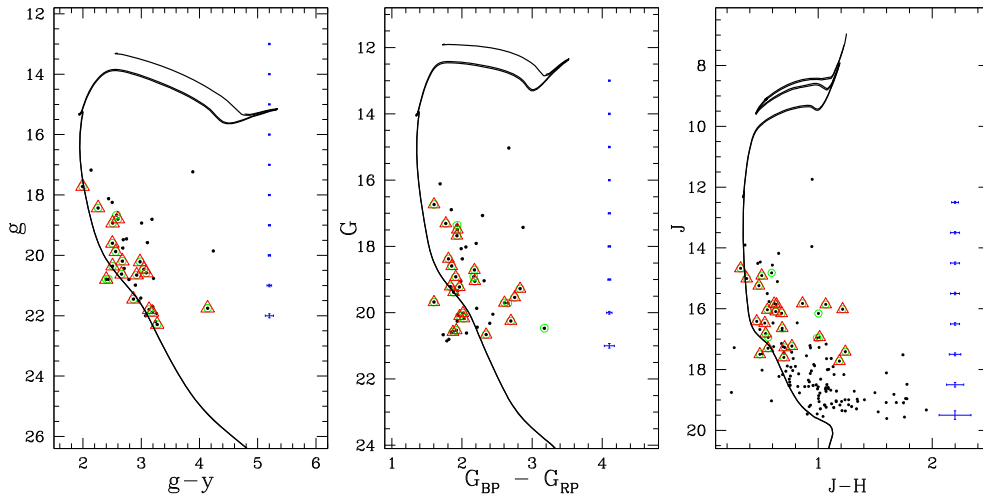


Figure 5. CMDs generated from PS1 (left panel), Gaia (middle panel) and TANSPEC data (right panel) for the stars in the cluster region. Symbols are same as in Figure 4. The black curve denotes an isochrone of age = 50 Myr derived from Pastorelli *et al.* (2019). The isochrone is corrected for distance (5.7 kpc) and extinction ($A_V = 3.95$ mag). Photometric error bars are also shown in CMDs.

Since the T76 cluster seems to be associated with a H II region, there might be a probability of finding young stars in it with excess IR emission. We have tried to find them using the conventional NIR color-based selection criteria (Sharma *et al.* 2007), but have found none. Therefore, to derive the age of the T76 cluster, we have used the deep multi-wavelength data from present observations, Gaia and PS1, to generate CMDs in different color spaces are shown in Figure 5. The CMDs display a well-defined MS and a MS turn-off point. We can visually fit an isochrone of age ~ 50 Myr (solid black curve) taken from Pastorelli *et al.* (2019) to the distribution of stars in the post-MS phase in all the CMDs. We are expecting 20% error in this age estimation (see e.g., Phelps & Janes 1994).

From the above analysis, it seems that the cluster T76 is located at a farther distance of 5.7 ± 1.0 kpc and is having an age of $\sim 50 \pm 10$ Myr.

3.4 Mass function

Open clusters possess many favorable characteristics for MF studies, e.g., clusters contain almost coeval set of stars at the same distance with the same metallicity; hence, difficulties such as complex corrections for stellar birth rates, life times, etc., associated with determining the MF from field stars are automatically removed. The MF is often expressed by a power law, $N(\log m) \propto m^\Gamma$ and the slope of the MF is given as:

$$\Gamma = d \log N(\log m) / d \log m, \quad (5)$$

where $N(\log m)$ is the number of stars per unit logarithmic mass interval. The MS luminosity function (LF) obtained with the help of g vs. $(g - i)$ CMD generated from the deep PS1 photometric data (cf. Figure 6) and corrected for the data incompleteness, has been converted into an MF using the isochrone of Pastorelli *et al.* (2019) of age ~ 50 Myr, corrected for the distance and extinction (see also Sharma *et al.* 2020, and references therein).

In Figure 6, we show the CMD for the cluster region as well as for the reference region (α_{J2000} : $22^{\text{h}}28^{\text{m}}08^{\text{s}}.4$, δ_{J2000} : $+61^{\circ}34'40''.7$) having the same area. The contamination due to field stars is greatly reduced by selecting a sample of stars which are located near the well-defined MS (cf. Sharma *et al.* 2008). Therefore, we generated an envelope of ± 0.5 mag around the CMD keeping in mind the distribution of member stars and is shown in the left panel of Figure 6. As the MS is extended from ~ 17.15 mag ($\sim 5.1 M_\odot$) to ~ 22.35 mag ($\sim 1.2 M_\odot$), the number of probable cluster members were obtained by subtracting the contribution of field stars (corrected for data incompleteness), in different magnitude bins having size of 1.0 mag from the contaminated sample of MS stars (also corrected for data incompleteness). We have used the estimation of the completeness factor (CF) for the PS1 data as has been estimated in our previous paper, i.e., Sharma *et al.* (2020). The photometric data is 90% complete up to 21.6 mag in the g -band, which corresponds to a star of mass $1.5 M_\odot$ at the distance of T76 cluster. We have also shown the MS turn-off point and 50% complete-

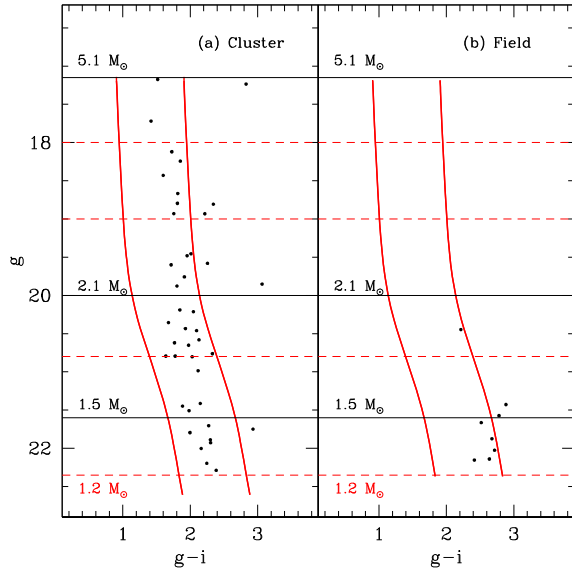


Figure 6. PS1 g vs. $(g - i)$ CMDs for the stars in the (a) cluster and (b) field regions. The curves denote a MS envelope created by the MS isochrone of 50 Myr derived from [Pastorelli et al. \(2019\)](#) corrected for the distance (5.7 kpc) and extinction ($A_V = 3.95$ mag) (see text for details). Upper and lower horizontal lines represent the MS turn-off point and 50% completeness limit, respectively.

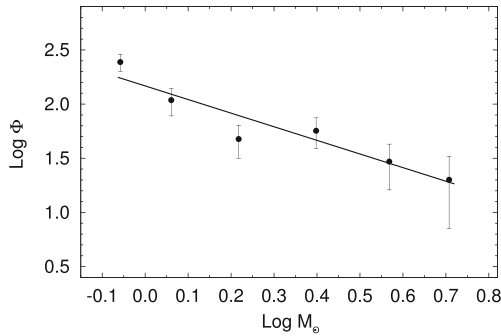


Figure 7. A plot of the MF for the cluster region of T76 using PS1 data. $\text{Log } \phi$ represents $\log(N/d \log m)$. The error bars represent $\pm\sqrt{N}$ errors. The solid line shows the least squares fit to the MF distribution (black filled circles).

ness limit in Figure 6. The resultant MF distribution for the cluster region is shown in Figure 7. The slope of the MF (Γ) in the mass range $\sim 1.5 < M/M_\odot < 5.1$ comes out to be -1.6 ± 0.3 for the stars in the T76 cluster region.

We have also used the present deep NIR photometry taken from the TANSPEC to derive the MF slope of the T76 cluster. The CF is determined for J vs. $J - H$ CMD using the same procedure as discussed in [Sharma et al. \(2020\)](#) and is shown in the top panel of Figure 8. To decontaminate the field star population, we have used

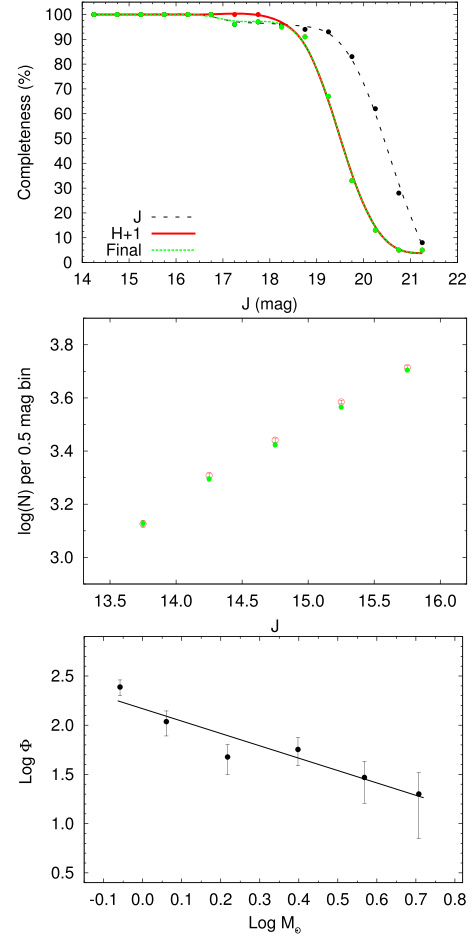


Figure 8. Top panel: The completeness factor as a function of J magnitude derived from the artificial star experiments (ADDSTAR, see [Sharma et al. \(2020\)](#) for details) on the TANSPEC J and H band images. The H -band completeness factor is off-set by the mean color of the MS stars (i.e., 1.0 mag). The continuous curves are the smoothed Bèzier curves for the data points for completeness. Middle panel: A comparison of field stars distribution generated by using a nearby reference field (green filled circles) and by the model/simulations generated by the Besançon model (red open circles). Bottom panel: A plot of the MF for the T76 cluster using TANSPEC data. $\text{Log } \phi$ represents $\log(N/d \log m)$. The error bars represent $\pm\sqrt{N}$ errors. The solid line shows the least squares fit to the MF distribution (black filled circles).

the CMD of a nearby reference field taken from the 2MASS survey (for stars having $J < 16$ mag) and the Besançon Galactic model of stellar population synthesis ([Robin et al. 2003](#); [Ojha et al. 2004](#)) (for stars having $J > 16$ mag). To check the accuracy of statistics of number of stars generated by the Besançon model, we have compared the LF generated from the model with that from the 2MASS survey ($J < 16$ mag) in the middle panel of Figure 8. The LFs from both methods

are matching well and the resultant MF distribution is shown in the bottom panel of Figure 8. The value of the MF slope (Γ) for the T76 cluster estimated by using the deep TANSPEC data, is -1.3 ± 0.2 in the mass range of $\sim 0.75 < M/M_{\odot} < 5.8$.

4. Discussion

Using our deep NIR data, the MF slope up to $0.75 M_{\odot}$ is found to be $\Gamma = -1.3 \pm 0.2$ for the cluster region, which is very similar (i.e., $\Gamma = -1.35$) to that reported by Salpeter (1955). This indicates that the distribution of stars in this cluster is similar to the distribution found in our solar neighborhood and the low mass stars are still intact with the cluster and there is no effect of dynamical evolution on them as of now. To further check this, we have used Allison *et al.* (2009) method to calculate mass segregation ratio (MSR) as a measure to identify and quantify mass segregation in the cluster. This method works by constructing the minimal sampling tree (MST) for massive stars and for the equal number of randomly selected stars from the cluster sample and estimating the ratio of their mean edge length, Γ_{MSR} (see for details, Olczak *et al.* 2011; Dib *et al.* 2018; Sharma *et al.* 2020). We have used the magnitudes of member stars (cf. Section 3.4) as a proxy for the mass. This avoids uncertainties when we convert the observed luminosities into masses (Dib *et al.* 2018). For the T76 cluster, we have estimated the value of Γ_{MSR} as 0.9 ± 1.7 , which dissuades the effect of mass-segregation in this cluster (see also, Sharma *et al.* 2020). A value of $\Gamma_{\text{MSR}} \approx 1$ implies that both samples of stars (i.e., the most massive and the randomly selected) are distributed in a similar manner, whereas $\Gamma_{\text{MSR}} > 1$ indicates mass segregation and $\Gamma_{\text{MSR}} \ll 1$ points to inverse mass segregation, i.e., the massive stars are more spread outwards than the rest.

To confirm the dynamical state of this cluster, we have estimated the dynamical relaxation time, T_E , the time in which the individual stars exchange sufficient energy so that their velocity distribution approaches that of a Maxwellian equilibrium, using the method given by Binney & Tremaine (1987). By counting the number of member stars (71 stars, cf. Section 3.4), the value of T_E comes out to be ~ 12 Myr for the T76 cluster (see also, Sharma *et al.* 2020). If we assume loss of 50% of stars due to incompleteness of our data, the dynamical relaxation time will be $T_E \sim 20$ Myr, which is only 2.5 times less than that of the estimated age of T76 cluster (50 Myr). This indicates that T76 cluster is still under the process of dynamical relaxation. Usually the low-mass member stars become the most vulnerable to be ejected

out of the system due to the dynamical relaxation, i.e., stellar evaporation happens with an e-folding time scale of $\tau_{\text{evap}} \sim 100 \times T_E$ (Shu 1982; Mathieu 1984; Binney & Tremaine 1987). As τ_{evap} comes out to be ~ 1 Gyr for T76 having age ~ 50 Myr, we can safely assume that the low mass stars have not ejected out of the cluster due to dynamical relaxation and the MF slope, which we have estimated is very much representative of the primitive IMF of the clusters. The typical survival time scale of open clusters in the galactic disk is about 200 Myr (Bonatto *et al.* 2006; Yang *et al.* 2013). Open clusters much older than the survival timescale usually have distorted shape and loosened structure, which lead to their disruption. The disintegrated open clusters will then become moving groups and supply field stars (Tang *et al.* 2019).

The structure of the star cluster depends on various processes, such as star formation, gas expulsion, dynamics of the cluster, etc. (Gutermuth *et al.* 2005). From the isodensity contours (cf. Section 3.1), we have found that the T76 cluster is showing more or less circular morphology, therefore, to further quantify the structure of this cluster, we have estimated the Q parameter (refer for details, Sharma *et al.* 2020) for the sample of cluster members. The Q parameter is generally used to distinguish between clusters with a central density concentration and hierarchical clusters with a fractal substructure (cf. Cartwright & Whitworth 2004, 2009). A group of points distributed radially will have a high Q value ($Q > 0.8$), while clusters with a more fractal distribution will have a low Q value ($Q < 0.8$) (Cartwright & Whitworth 2004; Chavarría *et al.* 2014). We have estimated $Q = 0.9$ for the T76 cluster, which is an indicative of the radial distribution of stars in this cluster. This is in agreement with our isodensity contour structures having circular geometry. As the cluster is still under the process of dynamical evolution, this radial distribution of the stars in the T76 cluster may be due to the star-formation process itself.

5. Summary and conclusion

We have performed a detailed analysis of the T76 open cluster using deep NIR observations taken with the TANSPEC on the 3.6m DOT along with the recently available high quality PM data from the Gaia DR3 and deep photometric data from PS1. We have investigated the structure of this cluster, determined the membership probability of stars in the cluster region, derived the fundamental parameters of the cluster, and studied the MF and mass segregation in this cluster. The main results of this study can be summarized as follows:

- We have found that the T76 cluster is showing an central density concentration with circular morphology using the isodensity contours and the Q parameter value. This distribution is most probably due to the star-formation processes. The radius of the T76 cluster is found to be $45''$ (1.24 pc at a distance of 5.7 kpc) centered at α_{2000} : $22^{\text{h}}28^{\text{m}}46^{\text{s}}.68$, δ_{J2000} : $+61^{\circ}38'01''.2$.
- Using Gaia DR3 data, 28 stars were marked as highly probable cluster members. We have estimated the distance of this cluster using both parallax of member stars and the isochrone fitting technique, and found that the cluster is located at a distance of 5.7 ± 1.0 kpc. We have also estimated the age of this cluster as 50 ± 10 Myr.
- We have derived the MF slope (Γ) in the cluster region in the mass range of $\sim 0.75 < M/M_{\odot} < 5.8$ as -1.3 ± 0.2 using our deep NIR data, which is similar to the value -1.35 given by Salpeter (1955). The cluster does not show any signatures of mass-segregation and is found to be undergoing dynamical relaxation.

Acknowledgements

We thank the staff at the 3.6 m DOT, Devasthal (ARIES) and IR astronomy group at TIFR, for their cooperation during TANSPEC observations. This work has made use of data from the European Space Agency (ESA) mission (Gaia, <https://www.cosmos.esa.int/gaia>), processed by the Gaia Data Processing and Analysis Consortium (DPAC, <https://www.cosmos.esa.int/web/gaia/dpac/consortium>). Funding for the DPAC has been provided by national institutions, in particular, the institutions participating in the Gaia Multilateral Agreement. This publication also makes use of data from the Two Micron All Sky Survey, which is a joint project of the University of Massachusetts and the Infrared Processing and Analysis Center/California Institute of Technology, funded by the National Aeronautics and Space Administration and the National Science Foundation. Part of the work/analysis was done at the National Astronomical Research Institute of Thailand. SS acknowledged the support of the Department of Science and Technology, Government of India, under project no. DST/INT/Thai/P-15/2019. DKO acknowledged the support of the Department of Atomic Energy, Government of India, under project no. RTI 4002.

References

- Allison R. J., Goodwin S. P., Parker R. J., *et al.* 2009, MNRAS, 395, 1449
- Anderson L. D., Armentrout W. P., Johnstone B. M., *et al.* 2015, ApJS, 221, 26
- Bailer-Jones C. A. L., Rybizki J., Fouesneau M., Demleitner M., Andrae R. 2021, AJ, 161, 147
- Binney J., Tremaine S. 1987, Galactic dynamics (Princeton, NJ: Princeton University Press)
- Bonatto C., Kerber L. O., Bica E., Santiago B. X. 2006, A&A, 446, 121
- Cantat-Gaudin T., Jordi C., Vallenari A., *et al.* 2018, A&A, 618, A93
- Cartwright A., Whitworth A. P. 2004, MNRAS, 348, 589
- Cartwright A., Whitworth A. P. 2009, MNRAS, 392, 341
- Chambers K. C., Magnier E. A., Metcalfe N., *et al.* 2016, arXiv e-prints. [arXiv:1612.05560](https://arxiv.org/abs/1612.05560)
- Chavarría L., Allen L., Brunt C., *et al.* 2014, MNRAS, 439, 3719
- Cutri R. M., Skrutskie M. F., van Dyk S., *et al.* 2003, VizieR Online Data Catalog, 2246, 0
- Dib S., Schmeja S., Parker R. J. 2018, MNRAS, 473, 849
- Fich M., Blitz L. 1984, ApJ, 279, 125
- Fich M., Treffers R. R., Dahl G. P. 1990, AJ, 99, 622
- Foster T., Brunt C. M. 2015, AJ, 150, 147
- Gaia Collaboration, Prusti T., de Bruijne J. H. J., *et al.* 2016, A&A, 595, A1
- Gaia Collaboration, Brown A. G. A., Vallenari A., *et al.* 2018, A&A, 616, A1
- Girard T. M., Grundy W. M., Lopez C. E., van Altena W. F. 1989, AJ, 98, 227
- Golay M. 1974, Introd Astron Photom <https://doi.org/10.1007/978-94-010-2169-2>
- Green G. M., Schlafly E., Zucker C., Speagle J. S., Finkbeiner D. 2019, ApJ, 887, 93
- Gutermuth R. A., Megeath S. T., Myers P. C., *et al.* 2009, ApJS, 184, 18
- Gutermuth R. A., Megeath S. T., Pipher J. L., *et al.* 2005, ApJ, 632, 397
- Kharchenko N. V., Piskunov A. E., Schilbach E., Röser S., Scholz R. D. 2016, A&A, 585, A101
- Kim I.-J., Pyo J., Jeong W.-S., *et al.* 2018, ApJS, 238, 28
- Kronberger M., Teutsch P., Alessi B., *et al.* 2006, A&A, 447, 921
- Kumar B., Omar A., Maheswar G., *et al.* 2018, Bull de la Soc R des Sci de Liege, 87, 29
- Lada C. J., Lada E. A. 2003, ARA&A, 41, 57
- Mathieu R. D. 1984, ApJ, 284, 643
- Ojha D. K., Tamura M., Nakajima Y., *et al.* 2004, ApJ, 616, 1042
- Olczak C., Spurzem R., Henning T. 2011, A&A, 532, A119
- Pandey A. K., Sharma S., Kobayashi N., Sarugaku Y., Ogura K. 2020a, MNRAS, 492, 2446
- Pandey R., Sharma S., Panwar N., *et al.* 2020b, ApJ, 891, 81

- Pandey R., Sharma S., Dewangan L. K., *et al.* 2022, *ApJ*, 926, 25
- Pastorelli G., Marigo P., Girardi L., *et al.* 2019, *MNRAS*, 485, 5666
- Phelps R. L., Janes K. A. 1994, *ApJS*, 90, 31
- Pineault S., Joncas G. 2000, *AJ*, 120, 3218
- Robin A. C., Reylé C., Derrière S., Picaud S. 2003, *A&A*, 409, 523
- Russeil D., Adami C., Georgelin Y. M. 2007, *A&A*, 470, 161
- Salpeter E. E. 1955, *ApJ*, 121, 161
- Sharma S., Pandey A. K., Ogura K., *et al.* 2006, *AJ*, 132, 1669
- Sharma S., Pandey A. K., Ogura K., *et al.* 2008, *AJ*, 135, 1934
- Sharma S., Pandey A. K., Ojha D. K., *et al.* 2007, *MNRAS*, 380, 1141
- Sharma S., Pandey A. K., Ojha D. K., *et al.* 2017, *MNRAS*, 467, 2943
- Sharma S., Ghosh A., Ojha D. K., *et al.* 2020, *MNRAS*, 498, 2309
- Sharma S., Ojha D. K., Ghosh A., *et al.* 2022, *PASP*, 134, 085002
- Shu F. H. 1982, *The Physical Universe* (Mill Valley, CA: University Science Books)
- Tang S.-Y., Pang X., Yuan Z., *et al.* 2019, *ApJ*, 877, 12
- Yadav R. K. S., Sariya D. P., Sagar R. 2013, *MNRAS*, 430, 3350
- Yang S.-C., Sarajedini A., Deliyannis C. P., *et al.* 2013, *ApJ*, 762, 3